이학석사 학위논문

Comparative analysis of changes in physical properties and intracellular composition of various cells using label-free optical diffraction tomography

울 산 대 학 교 대 학 원

의 과 학 과

조 민 주

Comparative analysis of changes in physical properties and intracellular composition of various cells using label-free optical diffraction tomography

지도교수 김준기

이 논문을 이학석사 학위 논문으로 제출함

2023년 08월

울 산 대 학 교 대 학 원

의 과 학 과

조 민 주

조민주의 이학석사학위 논문을 인준함

심사위원 백 찬 기 (인)

심사위원 탁 은 영 (인)

심사위원 김 준 기 (인)

울 산 대 학 교 대 학 원

2023년 08월

Abstract

Label-free optical diffraction tomography (ODT) enables the observation of cells and cellular organelles without the need for fluorescent labels or other preprocessing. It overcomes the constraints associated with conventional cell imaging techniques like fluorescence microscopy or electron microscopy. In the case of electron microscopy or fluorescence microscopy, which provide 2D images, a preprocess of the cell is necessary, which can induce cell invasion and cause changes in the physical and chemical composition inside the cell compared to live cells. However, ODT provides 3D images of cells and cellular organelles, as well as physical parameters such as refractive index, volume, and dry mass, allowing for the characterization of microenvironment changes within cells and internal biological properties without any preprocess applying on cell. In addition, when observing cells with ODT, Various preprocess on cell such as cell fixation, gene modification, immunofluorescence, and various cell trackers for biomarker can be applied to observe cells in different condition. With these preprocess, physical parameters obtained from ODT distinguish various types of cells under different conditions. Label-free cells and cells subjected to various manipulations undergo changes in both morphology and internal composition, which can be quantitatively evaluated through RI rendering by converting these changes into numerical values. Utilizing the advantages of ODT, observation of cells enables the discrimination of physical characteristics between similar cell categories in a live state. Additionally, specific markers within cells can be targeted through labeling, resulting in internal changes that can be quantitatively evaluated. In this study, numeric parameters such as the refractive index and volumes of human stem cells, fibroblasts cell, and HeLa cells were measured using ODT. Differences in refractive index caused by various physical stimuli, such as temperature, cell fixation, GFP protein tagging, and organelle tracking, were also compared. Three types of stem cells (hLD-SCs, hUCM-MSCs, and hiPSC) were campared to fibroblasts. The results revealed that stem cells exhibited widely distributed vesicles with larger volumes and higher mean RI values compared to fibroblasts. After cell

fixation and an increase in temperature, a significant overall decrease in the refractive index (RI) value of organelles, such as the nucleus and cytoplasm, was observed. Interestingly, while the RI values of cell nuclei were affected, the RI values of the cytoplasm were barely detected after membrane permeation. Moreover, the expression of GFP and GFP-tagged proteins was found to markedly increase the RI values of organelles in live cells, demonstrating more effective changes in RI compared to chemical fluorescence staining for cell organelles. This method enables the identification of differences between cells without the need for specific biological markers and indirectly assesses the impact of external stimuli on cellular organelles and this information can serve as a valuable reference for future studies that employ other conventional microscopy techniques.

Contents

List of figures

List of tables

1. Introduction

Within the dynamic and limited space of live cells, organelles and molecules carry out vital biological functions. Cells can exhibit diverse properties and behaviors depending on their type, microenvironment, and physiological conditions, which can lead to changes in their morphology, gene expression, signaling pathways, and other cellular functions. In addition, various stimulators such as hormones, drugs, and cytokines can affect both somatic cells and stem cells. However, due to the differentiation process, stem cells may exhibit unique morphological and physical characteristics that differ from somatic cells, which can also be evaluated through biological experiments. Biological experiments such as gene modification, immunohistochemistry, and cell fixation can be invasive to cells, leading to changes in their shape or function. Fluorescence microscopy and electron microscopy are methods used to observe and analyze these changes in cell morphology or function. Advanced fluorescence techniques such as fluorescence correlation spectroscopy (FCS), single molecule detection (SMD) and confocal laser scanning microscopy (CLSM) are often used to obtain and analyze images of biomolecules or subcellular organelles to obtain biological and physical information such as the intracellular distribution and motility characteristics of target molecules [1,2,3]. These microscopy imaging and analysis techniques require cell pre-treatment processes such as chemical cell fixation, ultrathin sectioning, and fluorescent staining. Unlike electron microscopy, fluorescent methods require pre-treatment with fluorescent labeling to target specific molecules or subcellular organelles, but allow for direct observation of living cells without chemical fixation. Therefore, these microscopy methods are very useful for high-resolution observation of changes in the characteristics of molecules or organelles depending on the physiological conditions of cells, but have limitations as they involve invasive manipulations of cells. Additionally, confirmation of various biomarkers such as immunofluorescence using traditional microscopy techniques is a common method. However, the two-dimensional

imaging measurement using fixed cells can be invasive and phototoxic, thereby limiting the accurate determination of characteristic properties of individual cell organelles. Optical diffraction tomography (ODT) is a label-free bioimaging technique that obtains 2D holographic images from multiple directions without labeling and reconstructs 3D images of cells [4,5,6]ODT enables observation of the inside of live cells using a microscope and allows for quantitative analysis of cell properties such as dry weight and volume by calculating the optical parameters inside the cell. This enables the assessment of physical alterations that occur within cells in response to various stimuli or artificial manipulation applying on cell [7,8,9,10,11,12,13]. The refractive index (RI) of cells can be used as a physical parameter to measure changes in molecules within the body, as it is proportional to density. [14] In addition, by combining label-free single-cell penetration imaging techniques and refractive index tomography, it is possible to observe the internal structure of the body using fluorescence which overcomes the limitation of access to certain molecular information with no labeling biomarker. [8,15,16] Various cell treatments, such as immunostaining, gene overexpression, chemical fixation, and organic fluorescent dye use, can also be performed to observe cells using ODT. By observing cells in a label-free state with 3D RI values and cell volume, which cannot be obtained from conventional electron microscopes or advanced fluorescence microscopes, or by observing cells with various pre-treatments, it is possible to understand how biological treatment methods affect cells. Recent studies using ODT have analyzed the refractive index of living cells and fixed cells, demonstrating that the refractive index of cells or cell compartments decreases after being fixed with paraformaldehyde, and showing that the RI changes among various cell lines are different. However, it is still unclear what effects various cell manipulation methods have on cells or intracellular compartments beyond chemical fixation. In this study, label-free ODT and fluorescent correlation ODT analysis techniques were used to quantitatively investigate the physical characteristics and properties of different organ-derived stem cells compared to

fibroblasts, overcoming the limitations of traditional 2D bright field microscopy observations, and assessing the physiological information of stem cells. The effects of various cell manipulation methods on single-cell compartments using HeLa cells were also analyzed. The stem cells used in this study were human liver-derived stem cells (hLD-SCs), which have characteristics similar to those of multipotent stem cells (MSCs) including differentiation ability and immune suppression effects. However, hLD-SCs do not express CD34 marker commonly found in blood cell. [17,18,19] Furthermore, human umbilical cord-derived multipotent stem cells (hUCM-MSCs) were also investigated. These undifferentiated multipotent stem cells have the ability to undergo self-regeneration and differentiate into various cell types. hUCM-MSCs are widely employed in drug discovery and cell therapy research due to their therapeutic potential. [20]. Human induced pluripotent stem cells (hiPSCs) were also examined in the study. These cells, derived from adult somatic cells, hold great promise for clinical cell therapy applications. However, their unique characteristics and distinct physical properties in comparison to cells lacking self-regeneration functions are still not fully understood. These three different types of stem cells were used to investigate the refractive index (RI) and volume of vesicles and nuclei, compared to fibroblasts. HeLa cells were used to assess the impact on cell plasma membrane, nucleolus, cytoplasm/nucleoplasm, and peripheral nuclear envelope region by dividing them into four cellular compartments or structures. The refractive index of compartments is considered an important parameter that presents the characteristics of a single cell, and thus, four cellular compartments or structures were measured for their refractive index using methods such as temperature changes, cell fixation, gene expression and immunofluorescence. Along with the changes in temperature and chemical fixation, various gene transfection such as mRFP-B23, mEmerald-Lamin, mGFP+EGFR, mGFP and mGFP+mRF B23 with HeLa cell were observed for cellular changes. Furthermore, the refractive index of structures was evaluated by staining the internal structures of living cells

using GFP-tagged proteins or fluorescent organelle tracker. Fluorescent dyes, called organelle trackers, to directly stain specific organelles such as the plasma membrane, mitochondria, lysosome, and endoplasmic reticulum (ER), and then analyze the stained live cells under fluorescence microscopy.[21] These trackers are dyes that can permeate through cell membranes, making them less invasive to cells. Previous studies using ODT have examined the refractive indices of living and fixed cells, and have indicated that the refractive index of organelles or compartments may decrease when cells are fixed with paraformaldehyde. Additionally, the magnitude of observed RI changes has been found to vary among different cell lines. [22,23] In this study, biophysical characteristics of stem cells were compared to fibroblasts cells to understand the unique characteristics of stem cell, and various cell conditions and manipulations were evaluated along with gene expression and cell organelle tracker to compare which cell manipulation causes less invasion to cells. This approach will aid in understanding how different invasive manipulation methods affect the physicochemical properties of individual cells, specifically at the level of internal cellular structures. It will also contribute to the optimization of molecular and structural fluorescent probes, as well as provide reliable analysis for various cell imaging techniques.

2. Material and Methods

2.1 Cell Preparation

2.1.1 HeLa Cell

HeLa cells were cultured in a 5% CO2 incubator at a temperature of 37 degrees Celsius in DMEM with 1% penicillin and streptomycin and 10% FBS. For ODT observation, Hela Cells were cultured in Tomo dish containing microscope cover-glass(Tomocube,Daejeon,Korea) for ODT observation. HeLa cells are classified into categories of live cells, fixed cells, immunofluorescent staining, and genetic modification and various cell trackers. Label-free live cells were observed at two temperature conditions, 37ºC and 25ºC, in Dulbecco's PBS (Phosphate Buffered Saline) (Biowest, Nuaille´, France). For fixed cells, HeLa cells were fixed in 4% paraformaldehyde (T&I, Chuncheon, Korea) in 0.1 M PBS, washed with PBS, and observed at 25°C. [24, 25]. HeLa cells stably expressing GFP-LC3 were donated by Dr. T. Yoshimori at Osaka University in Japan.[26]

2.1.2 Human Stem Cell

hLD-SCs derived from human liver were cultured in a 5% CO2 incubator at a temperature of 37 degrees Celsius in DMEM/F-12 with 1% penicillin and streptomycin and 10% FBS.[27] hUCM-MSCs derived from human umbilical cord matrix were cultured in in a 5% CO2 incubator at a temperature of 37 degrees Celsius in DMEM/F-12 with 1% penicillin and streptomycin and 10% FBS. [28] hiP-SCs were derived from peripheral blood mononuclear cells (PBMCs) and cultured in StemMACS. Fibroblasts derived from human skin were cultured in in a 5% CO2 incubator at a temperature of 37 degrees Celsius in DMEM/F-12 with 1% penicillin and streptomycin and 10% FBS.[29] Stem cells and fibroblasts cells were cultured in Tomo dish containing microscope cover-glass (Tomocube,Daejeon,Korea) for ODT observation. The study followed the principles set

forth in the Declaration of Helsinki, and all research protocols were reviewed and approved by the Institutional Review Board (IRB) of Asan Medical Center, Korea.

2.2 Immunofluorescence staining

a monoclonal antibody against HSF4 (Invitrogen, Oregon, USA) at a 1:300 dilution at a 1:200 dilution was used. The secondary antibody for fluorescence was Alexa flour 488 (Life technologies, California, USA). Sodium citrate buffer with a pH of 6.0 and a concentration of 0.01M was used for washing, while antigen retrieval was achieved using 0.05% Tween 20 with 0.1% Triton x-100 in sodium citrate buffer [30, 31]. Counter staining was performed using DAPI (Invitrogen, Oregon, USA) at a 1:1000 dilution. PBS buffer was used for washing during the process of immunofluorescence staining

2.3 Fluorescent dyeing of organelles for live cell imaging

To observe each organelle within a single living cell, HeLa cells were cultured and observed using various organelle trackers such as nuclear staining reagent Mito-Tracker, and ER-Tracker Blue-White DPX with 1:2000 dilution (Invitrogen, Carlsbad, USA) and Hoechst 33342 with 1 drop/ml (NucBlue Live ReadyProbes Reagent, Invitrogen, Carlsbad, USA). Cells were treated for 15 minutes in 37 degree 5% Co2 incubator for tracker activation.

2.4 Plasmids

Plasmids expressing monomeric RFP-B23 (nucleophosmin) fusion protein (mRFP-B23), GFP-Lamin A fusion protein (GFP-LA), EGFR-GFP fusion protein (EGFR-GFP), and monomeric GFP (GFP) were previously described [1,2,10,32,33,34]. Plasmid structures were confirmed by sequencing. The plasmid constructs utilized for transfection were purified using the Plasmid DNA Midiprep Kit (Qiagen, Hilden, Germany).

2.5 Cell transfection

HeLa cells were cultured onto a Tomo-dish (Tomocube, Daejeon, Korea) for transient expression of GFP or GFP-tagged proteins. Gene-specific expression was induced in HeLa cells with Lipofectamine 3000 Transfection Reagent (Thermo Fisher Scientific, Waltham, Massachusetts) following the optimized protocol by the manufacturer. Fluorescent observations were performed 24 hours after transfection.

2.6 Label-free ODT and correlative fluorescence imaging with refractive index tomography

Label-free ODT was used as previously described [11,35]. The ODT technique involves reconstructing a three-dimensional tomography of a single HeLa cell using multiple 2D holograms taken from various angles [35]. Live cell ODT measurements were conducted at 25°C or 37°C in a 5% CO2 atmosphere along with a 532 nm laser source and the ODT microscope (HT-2H, Tomocube Inc., Daejeon, Korea) [6,7] The ODT microscope is composed of a light source, a sample modulation device, and an optical field detection device. It captures the amplitude and phase information of light that passes through the sample cell. Using a Mach-Zehnder interferometer, the system reconstructs three-dimensional images of the cell. The microscope also enables fluorescence imaging of sample cells in three RGB color channels in 2D or 3D form. The laser power and exposure time projected onto the sample cell were optimized to avoid negative effects on RI measurement. Detailed information on the optical setup of the ODT and fluorescence imaging systems is provided in Figure 1(a). To verify the capability and reliability of the system, a fluorescent microsphere (Polysciences Inc., Warrington, USA) with a known RI value and a diameter of 6 μm was used. [11,36] The axial optical resolutions of the ODT system were 1 μm and lateral optical resolution was 200 nm. 2D and 3D images with fluorescence were gained by the combination of the ODT device and the fluorescence

microscope. Hoechst 33342 and ER-tracker were excited through a 392 ± 12 nm emission filter and detected through a 432 ± 18 nm bandpass filter. GFP was excited through a 474 ± 14 nm emission filter and detected through a 523 ± 23 nm bandpass filter, while RFP and Mito-tracker were excited through a 575 ± 12 nm emission filter and detected through a 702 ± 98 nm bandpass filter. The RI values of DMEM, PBS, and distilled water media were measured at different temperatures with a refractometer (Abbemat 3200; Anton Paar GmbH, Graz, Austria) and served as reference RI values for ODT measurement. The resolution of RI value was <0.001 [8,36].

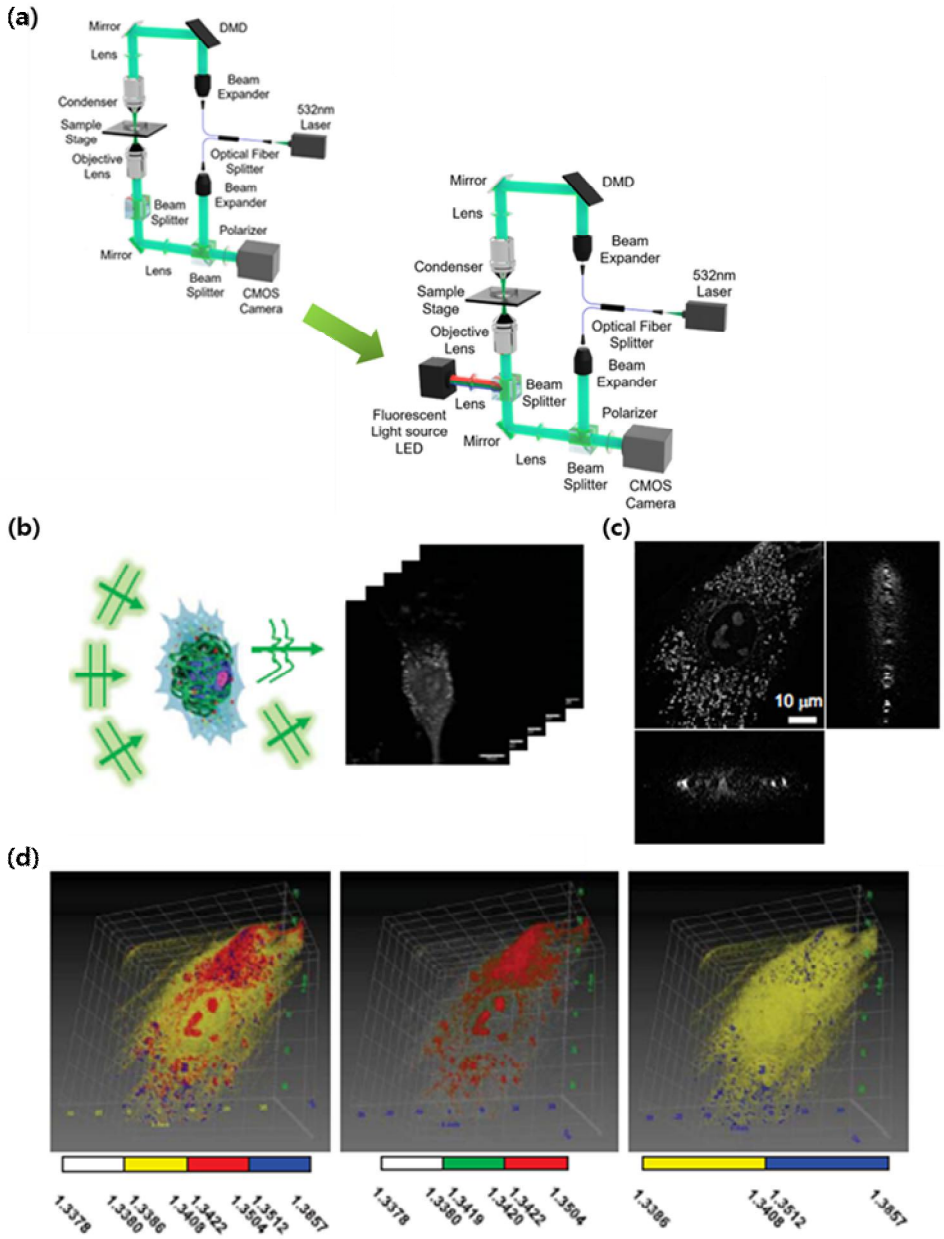

Figure 1. 3D ODT correlating with fluorescence setup and label free cell images (a) label free 3D ODT setup and total ODT setup with fluorescent light source for FL images (b) A diagram of 3D reconstruction involves obtaining a 2D hologram image using the reference light and scattered light. (c) cross-sectional slices of a 3D image(Scale bar=10 μm) in the x-y, x-z, and y-z plane of human stem cell, hUCM-MSC. (d) images with RI rendering using Tomocube studio program.

3. Results

Chapter 3.1. ODT measurement in human stem cell comparing with fibroblast

3.1.1 Acquisition of ODT images in human stem cell and fibroblast

Raw images of optical diffraction tomography (ODT) were used to obtain label-free 3D images of three types of stem cell such as hiPSC, hUCM-MSC, hLD-SC and fibroblasts. The refractive index (RI) mapping image showed different RI values for the vesicles, nucleolus, cytoplasm, and plasma membrane of each cell type and represented as images shown in Figure 2 a. Mean RI values of each organelle were calculated from the rendered RI images. The RI values of the cytoplasm and nucleoli of hLD-SC differ from the RI value of hiPSCs and fibroblasts. Additionally, the RI values of vesicles in hUCM-MSC, hLD-SC, and hiPSC were higher than in fibroblasts, which means that vesicles are a unique physiological properties of stem cells. The plasma membrane of each stem cells and fibroblast cells had the same RI value. Figure 2 b shows the mean volume of all cells. The volume calculation of individual hiPSC can be challenging due to their tendency to proliferate in colony formations. However, the distinct boundaries between the cytoplasm and nucleolus of each cell enable the evaluation of individual cells based on this criterion. Compared to the other cell types, single hiPSC exhibited a significantly smaller mean volume. There were no noticeable differences in single cell volume between hUCM-MSC and fibroblasts. However, the single cell volume of hLD-SC was approximately half that of hUCM-MSC and fibroblasts. These findings suggest that cell volume alone is not a major distinguishing characteristic of the two stem cell types. To further investigate the differences between these cells, the mean refractive index (RI) of nucleoli and vesicular structures (such as vesicles) was examined. The results showed that stem cells had higher mean RI values for these organelles compared to fibroblasts. Additionally, the volume and number of organelles within a single cell were analyzed to determine their volumetric and numeric

characteristics. Figure 2 c illustrates the comparison of mean cell volume across different cell types. While single cells were clearly distinguishable and analyzed for all cell types except for hiPSC, which formed colonies and required a calculation based on the nucleolus and cytoplasm. The mean volume of single hiPSC was found to be smaller than that of other cell types. There was no difference in single cell volume between hUCM-MSC and fibroblasts, but the single cell volume of hLD-SC was half that of hUCM-MSC and fibroblast. These results suggest that cell volume is not a significant. (Table 1)

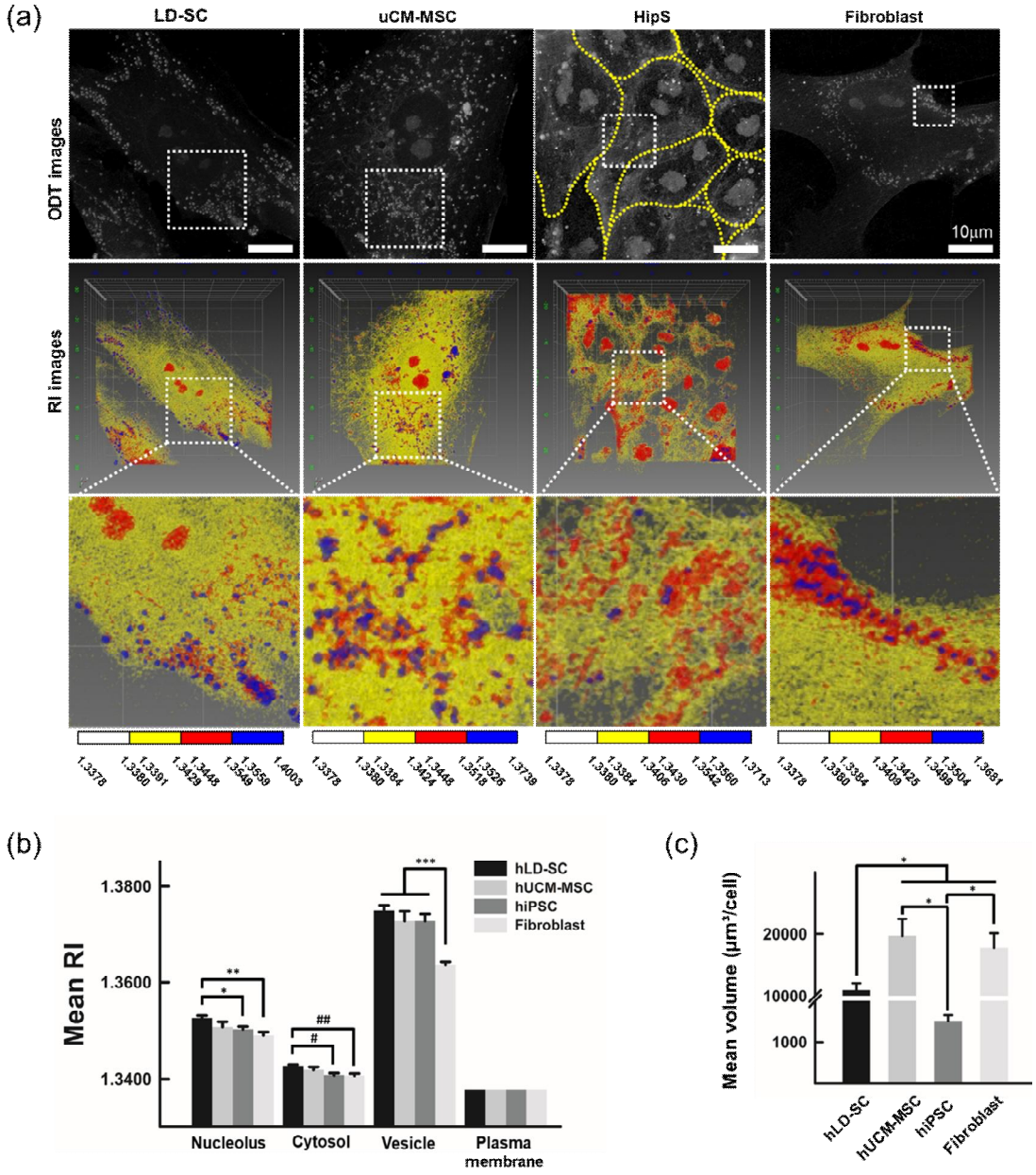

Figure 2. Label free live ODT image, Refractive Index and mean volume of three different types of stem cells and fibroblast cells (a) ODT raw Images of hLD-SC, hUCM-MSC, hiPSC and fibroblast (top), RI mapping Images, enlarged RI mapping for vesicular structure part (b) RI value of each organelle (nucleoli, vesicles, and plasma membrane). (c) Mean volume of fibroblast and each stem cell.

Table 1. Summary RI value of Cell density for each cellular organelles of Stem cell and fibroblast.

Cell Organelles and component	Cell Density(g/ml)			
	hLD-SC	**hUCM-MSC**	**hiPSC**	**Fibroblast**
Nucleolus	0.0950 ± 0.0027	0.0854 ± 0.0057	0.0828 ± 0.0030	0.0763 ± 0.0039
Cytosol	0.0447 ± 0.0013	0.0404 ± 0.0029	0.0357 ± 0.0018	0.0349 ± 0.0018
Vesicle	0.2059 ± 0.0058	0.1948 ± 0.0109	0.1949 ± 0.0077	0.1495 ± 0.0038
Plasma Membrane	0.0210	0.0210	0.0210	0.0210

3.1.2 Quantitative analysis of nucleoli and vesicles

The mean refractive index (RI) values of the organelles, such as vesicular structure and nucleoli, showed a clear difference between fibroblasts and stem cells. As stem cells has higher RI values compared to fibroblasts, the numeric and volumetric characteristics of these organelles were evaluated for each single cell to determine their properties. Label-free ODT images were reconstructed using IMARIS software to evaluate the numeric and volumetric characteristics of vesicles and nucleoli of different stem cells and fibroblasts in 3-demensional images. In the case of hiPSC, which proliferates by forming colonies, the cells was determined based on the number of nuclei counted. To calculate the average volume of nucleoli, the total volume was divided by the number of cells. Similarly, the mean number of vesicles per single cell was determined by dividing the total number of vesicles by the number of cells. On the other hand, the number of vesicles and nucleoli of hLD-SC, hUCM-MSC, and fibroblast were calculated for each single cell. The median volume of all stem cells and fibroblast cells was lower than the mean value. However, the mean volume of single vesicles in stem cells was significantly larger compared to that of fibroblasts, suggesting that the distribution of volume for single vesicles is right-skewed. (Table 2, Figure 3 b-e). hLD-SC and hUCM-MSC exhibited a larger number of vesicles and a larger volume compared to the rest cell types. The histograms represent the volume of single vesicles (Figure 3 b-f). Although due to limitations in current RI rendering techniques, conducting a quantitative analysis to determine the correlation between single vesicle volume and refractive index (RI) is difficult. However, it was observed that the mean RI value of hLD-SC, hUCM-MSC and hiPSC vesicles was higher compared to fibroblast vesicles. Moreover, vesicles with large volume were found to be extensively distributed, indicating that these characteristics were unique to the three stem cell types. cells. In contrast to the other two stem cell types, hiPSC vesicles exhibited a lower abundance of large-volume vesicles. Furthermore, hiPSCs exhibited a distinct characteristic in which the

ratio of nucleolus volume to the average cell volume was considerably larger than that of other cell types (Figure 3g). Additionally, the average number of vesicles per hiPSC was significantly lower compared to the rest cell types. (Figure. 3 f).

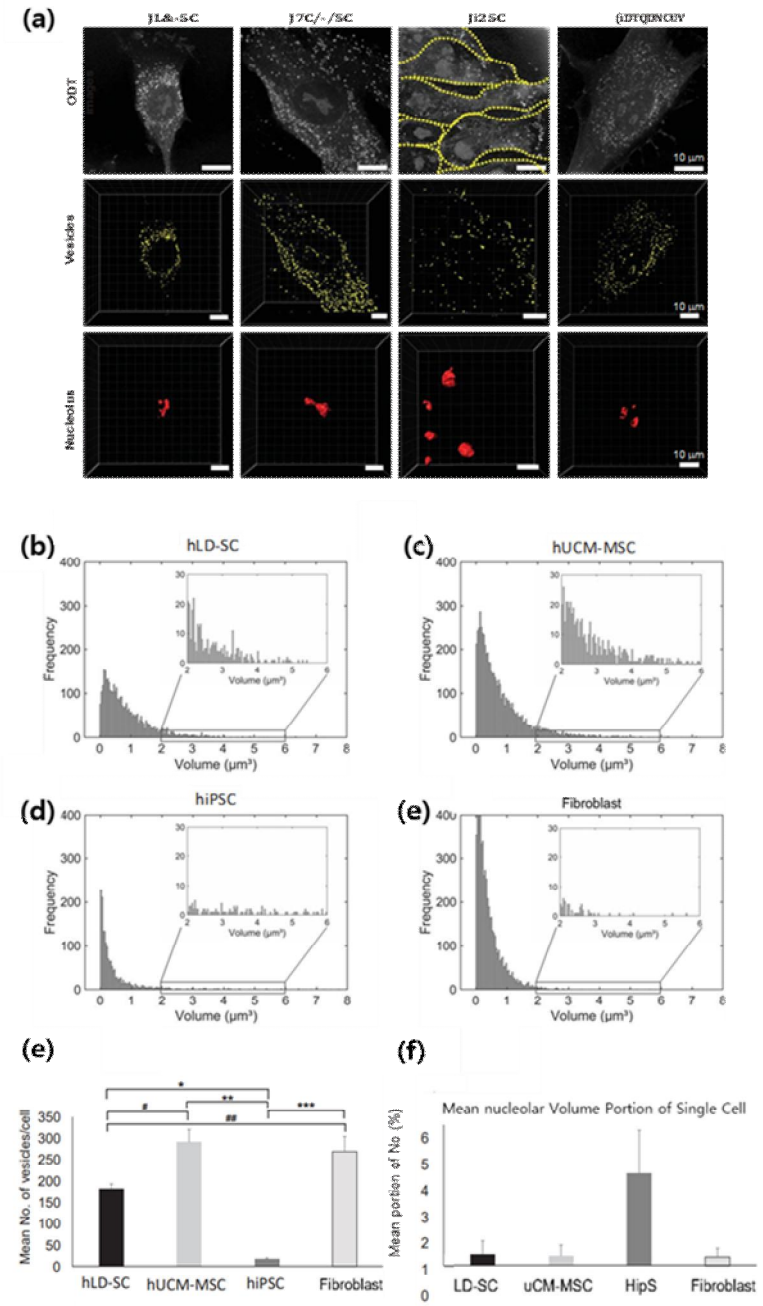

Figure 3. The result a label-free 3D ODT analyzing the vesicular structures and nucleoli in different cell types. a)3D ODT images and Vesicular structures and nucleoli of hLD-SC, hUCM-MSC, hiPSC, and fibroblasts reconstructed for numerical analysis. b) the histograms that presents volume of single vesicles in each cell type. c)The mean number of vesicles and nucleolar volume found in each cell calculated and presented in graph.

Table 2. Summary Mean volume of single vesicle for Stem cell and fibroblast

Mean Volume of single vesicle (µm3)				
	hLD-SC	**hUCM-MSC**	**hiPSC**	**Fibroblast**
Mean ± SD	0.8654 ± 0.0137	0.8307 ± 0.0119	1.0595 ± 0.1445	0.4272 ± 0.0059
Median	0.6357	0.5545	0.2366	0.2936

Chapter 3.2 Evaluation of the effect on HeLa cell under various cell manipulation

3.2.1 ODT image acquisition and evaluation of label-free or fluorescently labeled cells

A fluorescence microscopy-based ODT instrument is presented in Figure 1, which was used for label-free measurement of cells by acquiring multiple 2D holograms of human stem cell and HeLa cell at various illumination angles through a Mach–Zehnder interferometric microscope equipped with a digital micromirror device (DMD). The scattered light from the transparent cell interfered with the tile reference light, generating a spatially modulated hologram (Figure1 a). Phase images of the cell were obtained using a phase search algorithm (34; 35) to assemble an RI distribution by scanning sequential angles from 2D holograms. Figures 1(b) and (c) show 3D RI tomography reconstructed from several 2D hologram images. Previous studies have indicated that the nucleolus is expressed by three RI values and that the cytoplasm and nucleoplasm can be analyzed separately using different RI values [13, 10]. To compare the mean RI values of each organelle, this chapter divided the HeLa cell into four organelles with different RI ranges, namely the cell plasma membrane (PM), the nucleolus surrounded by the nuclear membrane (NO), the cytosol (Cyt), and the dense perinuclear region where the endoplasmic reticulum and mitochondria overlap (PNER) (Figure 1). There are several methods for fluorescently labeling cells in the field of cell biology, which can be broadly categorized into three types. To detect a target protein in cells through immunostaining, the cells first need to be fixed, and then the cell membrane should be permeabilized. Secondly, a genetic method of expressing a GFP-tagged target protein is employed for observing the distribution of a target protein in real time in living cells. Lastly, organelles such as nuclear DNA, mitochondria, Endoplasmic reticulum can be stained using organic dyes (i.e. fluorescence trackers) to observe the real-time behavior of living cells. The second and third methods are often used in conjunction. ODT measurement is performed on fluorescently labeled cells to obtain 2D- or 3D

fluorescence images within seconds. The objective lens is typically scanned along the Z-axis separately from the ODT system to acquire 3D fluorescence images. The RI rendered image of ODT and fluorescence image of a fluorescently labeled HeLa cell obtained sequentially in this way can be analyzed as a correlative ODT and fluorescence image. Although there is a difference of a few seconds from the acquisition of the ODT image till that of the fluorescence image, it is assumed that each organelle does not move significantly compared to the size of cells and organelles. The correlative ODT and fluorescence image is useful for comparing the fluorescence images of each labeled organelle and GFP-tagged proteins with the RI rendered images, and for determining whether cells are properly stained based on the method used.

3.2.2 Effect of temperature, cell fixation, and membrane permeabilization organelles.

HeLa cells were observed under various conditions to investigate the effects of temperature change from 37 to 25℃, chemical fixation using 4% paraformaldehyde (PFA), and cell permeabilization with 0.1% Triton X-100 on the four cellular regions. RI rendered images of each condition in HeLa cell are displayed in Figure 4 a-d. Previous studies have often combined chemical fixation with fluorescence staining and antibody permeabilization to examine the effects on the physical properties of cells. In this experiment, the objective was to investigate whether temperature variations have differential effects on organelles. Fluorescent imaging is typically performed at 25℃ to avoid mechanical vibration, but it is unclear how this affects organelles. The results showed that while the morphology of cells did not change significantly between temperatures, the refractive index of each organelle increased as temperature decreased by 12 degrees (Figure 5.a). The refractive index of media solutions is known to be linearly proportional to temperature. [37; 36; 38]. The results showed that, as temperature decreased, the RI value of the PBS solution increased by 0.0015, whereas the organelles No and PNER exhibited significantly greater increases, by 0.0034 and 0.0029, respectively. Conversely, the RI values of the organelles Cyt and PM increased by similar amounts to the PBS solution, at 0.0014 and 0.0011, respectively. These findings suggest that high-density organelles, which have heterogeneous systems, are more sensitive to temperature changes than homogeneous systems such as solutions. A decrease in the refractive index of organelles in chemically fixed cells was also observed, even without morphological changes, when compared to living cells at room temperature (Figure 5 b). This decrease in RI values due to chemical fixation is consistent with the findings of a previous study [23] Previous studies have reported swelling of HeLa cells due to PFA fixation, which may cause a decrease in the RI value of organelles [19]. To further investigate the effects of cellular permeabilization using a typical detergent (0.1% Triton X-

100) and antibody immunostaining on organelles, it is found that cell permeabilization caused a significant reduction in overall intracellular density, including the plasma membrane. Specifically, the cytosol showed a large decrease in the RI value to the point where it was undetectable compared to the nucleolus, nucleoplasm, and PNER region (Figure 5 c). This result suggests that a significant number of soluble macromolecules in the cytoplasm were released from the cell. Morphologically, the PNER region of the immunostaining cells after permeabilization showed a significantly larger and more prominent shape compared to living cells or fixed cells (Figure 4 b,c). To obtain more detailed properties of the nucleus and nucleolus, Immunostaining was carried out for DNA, HSF4 (heat shock transcription factor 4) to confirm the normal distribution of nuclear proteins. The immunostaining for HSF4 confirmed their respective localization in the nucleoplasm and nucleolus, as previously reported [39; 40; 41]. It was confirmed that these nuclear and nucleolar proteins are well-preserved in their respective locations, despite the overall decrease in RI value in the nucleus and the morphological change of the nucleolus. This is likely to have occurred because the contrast of the PNER region was increased by the large decrease of the refractive index in the cytosol. Figure 5 summarizes the influence of temperature change, chemical fixation, and transmembrane manipulation on the mean RI value of the four intracellular organelles. The effect of temperature change and chemical fixation on the refractive index of organelles was found to be homogeneous, while cell permeabilization had a distinct and significant effect on organelles, particularly on the cytosol. Surface plasmon resonance imaging has shown that Triton X-100 permeabilization leads to the elimination of more cellular membrane lipids and a significant reduction in intracellular mass density [42]. Our results, which indicate a substantial loss of intracellular cytosolic components and a significant decrease in the overall refractive index of cells due to permeabilization, are consistent with the findings of this previous study obtained by surface plasmon resonance analysis.

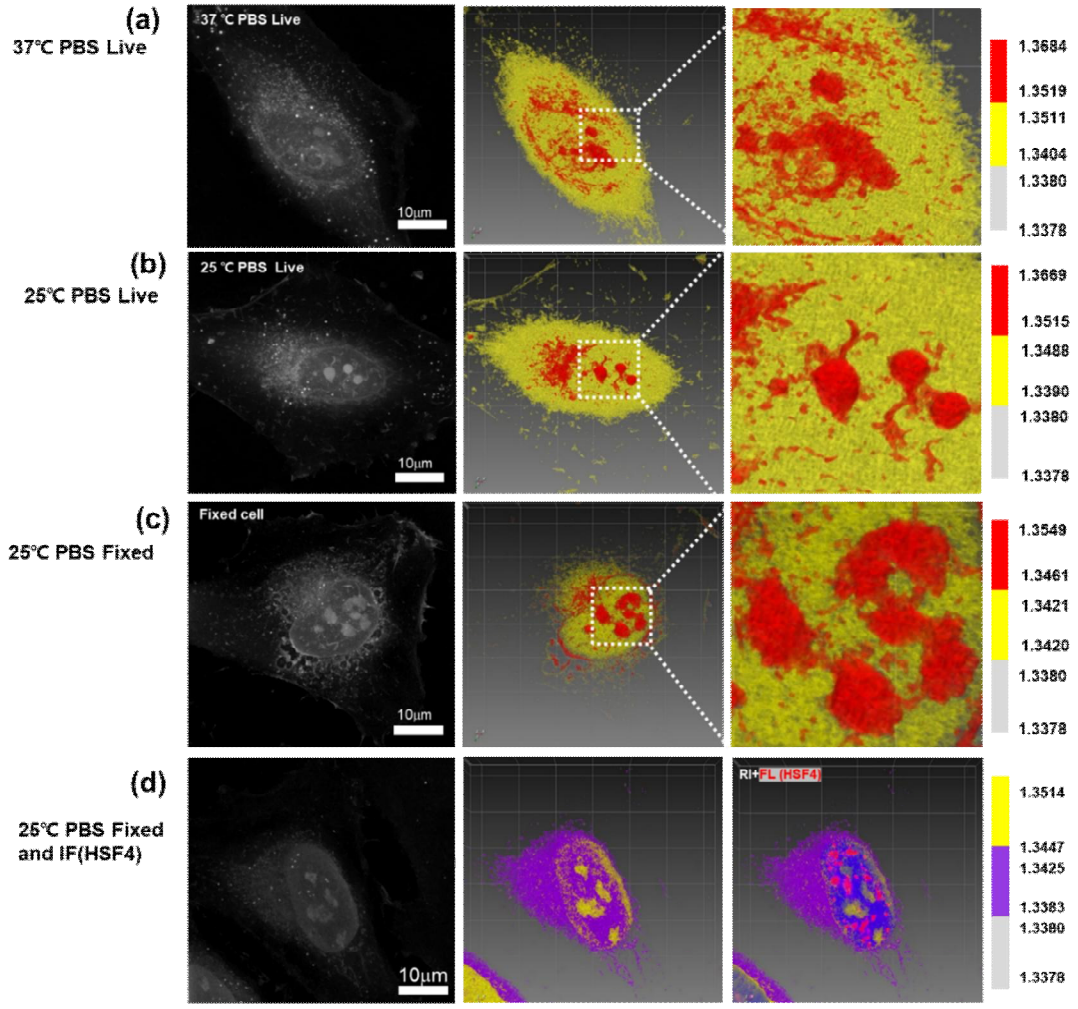

Figure 4. ODT raw image and RI rendered images of HeLa cells in different conditions. a) a single cell in PBS buffer at 37℃ b) at 25℃, c) cell fixed with 4% PFA d) immunofluorescence staining permeabilized with 0.1% Triton X-100. Immuno-stained cell also stained by Hoechst (blue) and HSF4 (red). The pseudo color bars indicate the RI ranges used for RI rendering. The abbreviations NO, PNER, Cyt, PM, FL, and RI represent the nucleolus, peri-nuclear ER region, cytoplasm, plasma membrane, fluorescence, and refractive index, respectively. The scale bars are 10 μm.

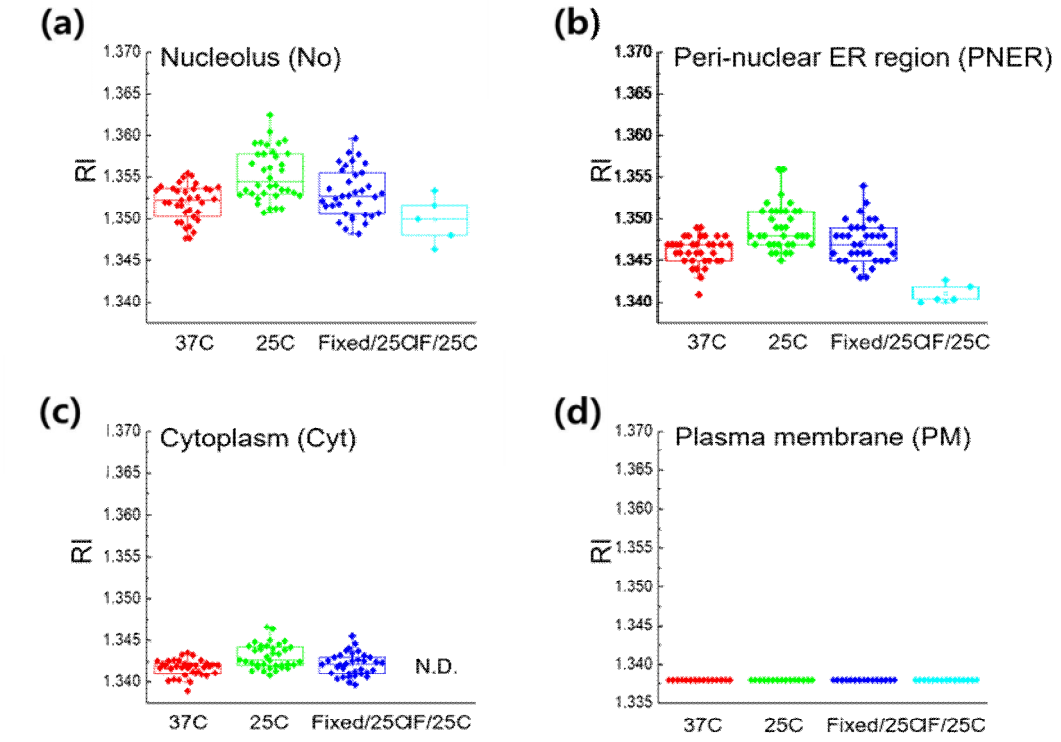

Figure 5. The RI values of different organelles in HeLa cells represented in graphs. Each cell was measured in PBS buffer under various conditions such as Temperature changes from 37℃ to 25℃, cell fixation with 4% PFA at 25℃ (Fixed/25C), and Immunofluorescence staining after cell permeabilization with 0.1% Triton X-100 measured at 25℃ (IF/25C) a) Nucleolus, b) Peri-nuclear ER region(PNER) (c) the cytosol (Cyt) (d) the cell plasma membrane (PM) are shown, respectively. N.D. indicates no detection.

3.2.3 Effect of transient gene overexpression on single HeLa cells

Microscopic imaging technologies have recently been used with genetically combine fluorescent proteins of various colors with target proteins and express them in single living cells to analyze intracellular distribution or dynamic characteristics of target proteins. The expression of the transfected genes can be detected within 24 hours after intracellular delivery of target genes using transfection reagents of cationic liposomes. Various methods of transfection have been developed, but the complete effects of these methods on cells and organelles are still not understood yet. In this experiment, the effect of transfection using the reagent of cationic liposome on HeLa cells was evaluated by comparing cells subjected to transfection with cells without manipulation (Figure 6), Subsequently, the effect of genetic overexpression of various fluorescent protein-tagged proteins after transient transfection on the refractive index of intracellular organelles was evaluated in RI values (Figure 7). HeLa cells expressing GFP-Lamin A were observed through ODT and found to be localized in both the nuclear membrane and nucleoplasm.[43] Similarly, EGFR-GFP was observed in the plasma membrane and peri-nuclear ER region[30], while mRFP-B23 was observed in the nucleolus[28,3](Figure 6). HeLa cells that express no morphological changes of the whole cell were detected in all conditions. The shape of the nucleolus is commonly observed to be round, but it remains unclear whether this change is caused by transfection or overexpression of GFP-tagged proteins. This uncertainty arises from the presence of cells in which the nucleolus is naturally round, even under normal conditions without transfection. In addition, when comparing mRFP-expressing cells to non-expressing HeLa cells, which were not transfected with mRFP but were from the same cell line, RI values were observed to increase in the nucleolus and PNER regions of the mRFP-expressing cells, but there was no significant difference in the cytosol. Therefore, it can be inferred that the transfected gene influences the density changes in the nucleus and PNER, which are key organelles for gene expression within the cell. The intracellular fluorescence distributions of

GFP-LA, EGFR-GFP, mRFP-B23, and GFP proteins were consistent with previous studies [1; 3; 43; 44]. The region of strong fluorescence intensity of the GFP/mRFP-tagged proteins localized in each specific organelle was well aligned with the region of high refractive index of the corresponding organelle (Figure 6 g). A high refractive index was detected in the region where the fluorescence intensity of EGFR-GFP was high in the cell membrane and PNER for cells expressing EGFR-GFP (Figure 6 e). When analyzing the refractive index specifically in the plasma membrane, it was found that the refractive index of the plasma membrane of cells expressing EGFR-GFP was much higher compared to cells without expression (Figure 6 e,f). Although the shape of the nucleolus is often round (Figure 6 e), it is unclear whether the effect was due to transfection or overexpression of GFP-tagged proteins because there were cells in which the nucleolus was round even under normal conditions without transfection. Regions adjacent to the plasma membrane with high refractive index are often present even in normal cells without overexpression of EGFR-GFP, making it difficult to consider it as an increase in refractive index due to the overexpression (Figure 7). This observation suggests that EGFR-GFP is mainly localized in the plasma membrane or in an area adjacent to the plasma membrane with a high density. There is no significant changes in refractive index value of the nucleolus and PNER by GFP-tagged proteins or overexpression of GFP. However, cells overexpressing EGFR-GFP or mRFP-B23 showed a significant increase in the refractive index within the cytosol, while the refractive index of the plasma membrane increased significantly only in cells overexpressing EGFR-GFP.

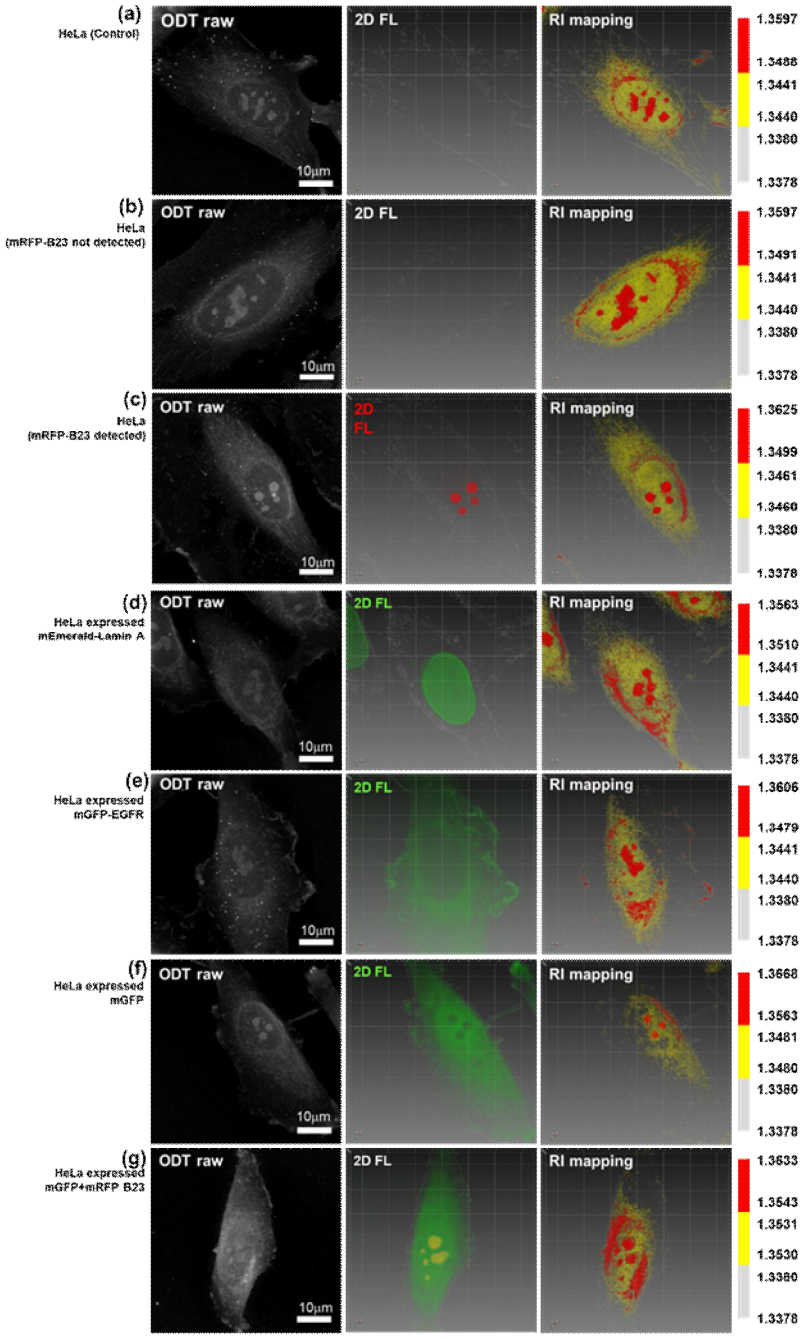

Figure 6. Raw RI Image of transient gene overexpression on single HeLa cell ODT measurements were performed on all cells in fresh DMEM media after 24 hours. a) HeLa control b) HeLa(mRFP-B23 not detected) c) HeLa(mRFP-B23 detected) d) HeLa(mEmerald-Lamin A) e) HeLa(mGFP+EGFR) f) HeLa (mGFP) g) HeLa expressed (mGFP+mRF B23) The scale bars are 10 μm

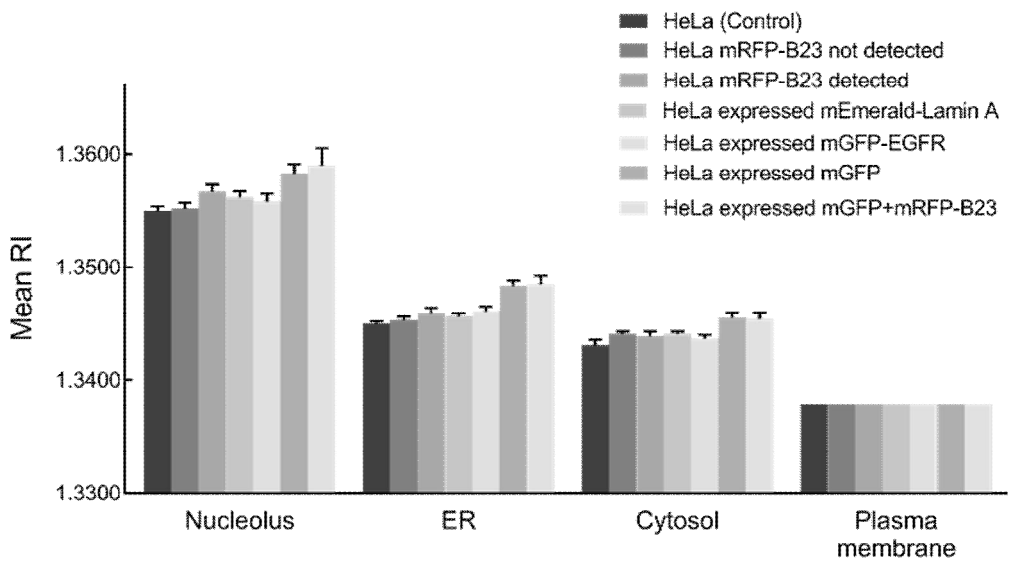

Figure 7. The refractive index (RI) values of four different cellular organelles in live HeLa cells with various gene transfection Nuclear membrane (NO), the dense perinuclear region of endoplasmic reticulum (PNER), the cytoplasm (Cyt), and the cell plasma membrane (PM)) in both normal and transfected HeLa cells. This graph shows that the averaged RI values differed among the different organelles and between the normal and transfected cells.

3.2.4 Influence of cell-permeable fluorescent trackers and stable expression of GFP-tagged LC3 on HeLa cells

Fluorescently staining specific organelles in living cells using organic dyes is also commonly used. These organic dyes, also called fluorescent trackers, are capable of specifically staining different organelles, such as Hoechst for nuclear DNA staining, ER-tracker for endoplasmic reticulum, Mito-tracker for mitochondria. The influence of these three fluorescence trackers on the physical properties of each organelle was analyzed. Additionally, the physical characteristics of HeLa cells expressing GFP-LC3 were compared to the results obtained from these fluorescent trackers (Figure 9). Unlike the transient transfection method using cation liposomes, cells stably expressing fluorescent proteins were analyzed in a state where the physicochemical stimulation to cells was minimized, and thus, they were compared to the membrane-permeable trackers, which also minimize external stimulation. HeLa cells stably expressing GFP-LC3, a marker protein of autophagosomes, are widely used in autophagy research. [26,45,46]. Among the fluorescent trackers, ER-tracker and Mito-tracker showed high fluorescence mainly in the PNER region together, indicating that the dense endoplasmic reticulum and mitochondria are intermingled in that region (Fig. 8 b,c). It is unclear which of the two organelles contributes more to the high density of PNER domains. However, the results support the formation of a PNER region with a high refractive index, as detected in ODT (Fig 9). Although mitochondria are also found in the PNER, their discontinuous and thin linear structure contribute less to the high-density structure compared to the continuous and sheet structure of the rough ER [55,56]. No morphological changes were shown in cells treated with each fluorescent tracker, and each fluorescent tracker represented the distribution of organelles based on the fluorescence intensity, as shown in Figure 8. Figure 9 provides a summary of the impact of fluorescence staining on organelles in live cells and GFP-LC3 HeLa cells, which express the GFP-LC3 protein, by measuring the refractive index values in each organelle. In HeLa

cells with Hoechst staining, the refractive index of the cytosol and nucleoli was significantly higher compared to control HeLa cells. However, no significant changes were observed in the refractive index of the other organelles. HeLa cells stably expressing GFP-LC3 had a smaller cell size compared to cells under other conditions, but the PNER region was dense and widely expanded toward the cytoplasm (Figure 8 d). The refractive index of each organelle was found to be relatively higher than normal cells. The fluorescence of GFP-LC3 is evenly distributed in the cytoplasm and nucleus at normal condition, which was consistent with previous studies [54,58]. Finally, HeLa cells that stably express GFP-LC3 showed an increase of refractive index in all organelles except the PNER. This result suggests that the approach of stably expressing a GFP-tagged protein leads to significant alterations in the physicochemical properties of organelles, as compared to transient overexpression or chemical fluorescent modification of organelles with GFP-tagged proteins.

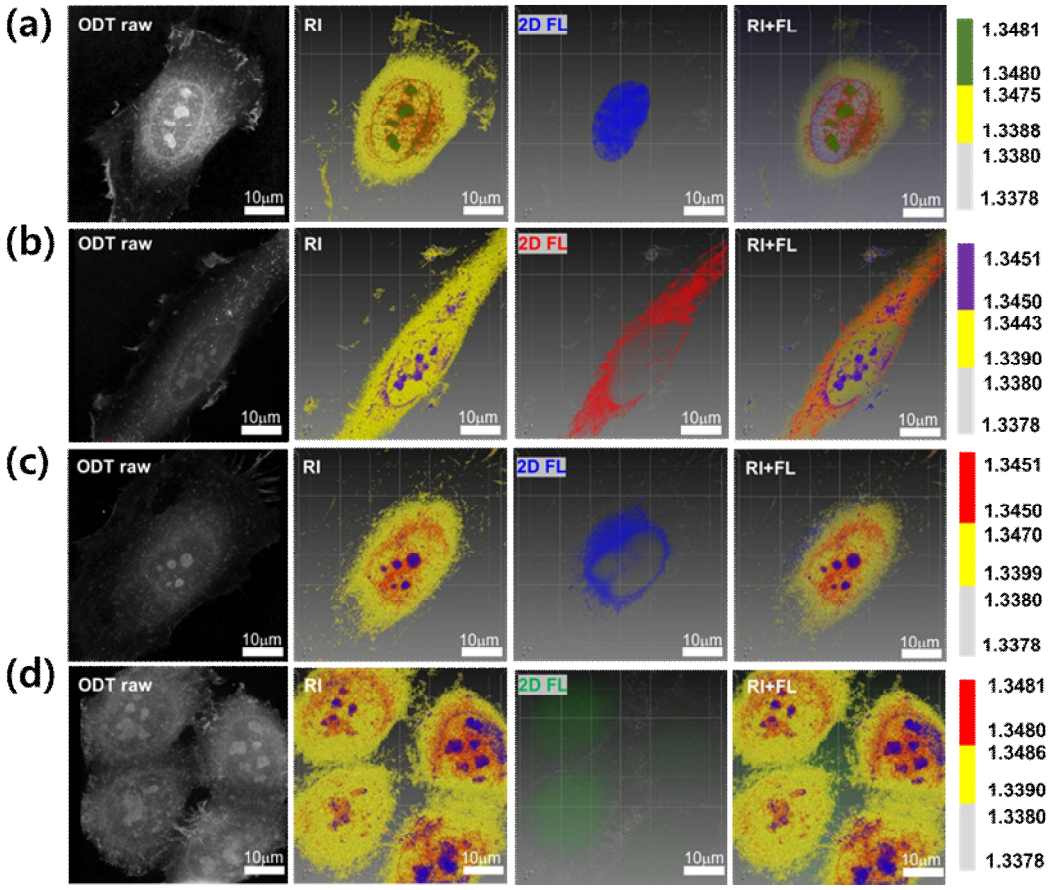

Figure 8. Raw ODT images and rendered images of four different cellular organelles in live HeLa cells with various fluorescence organelle tracker HeLa cells were treated various fluorescence organelle tracker for 15 mins in 5% Co2 37°C incubator a) Hoechst b) Mitochondria c) Endoplasmic Reticulum d) LC3-GFP transient expression HeLa cell

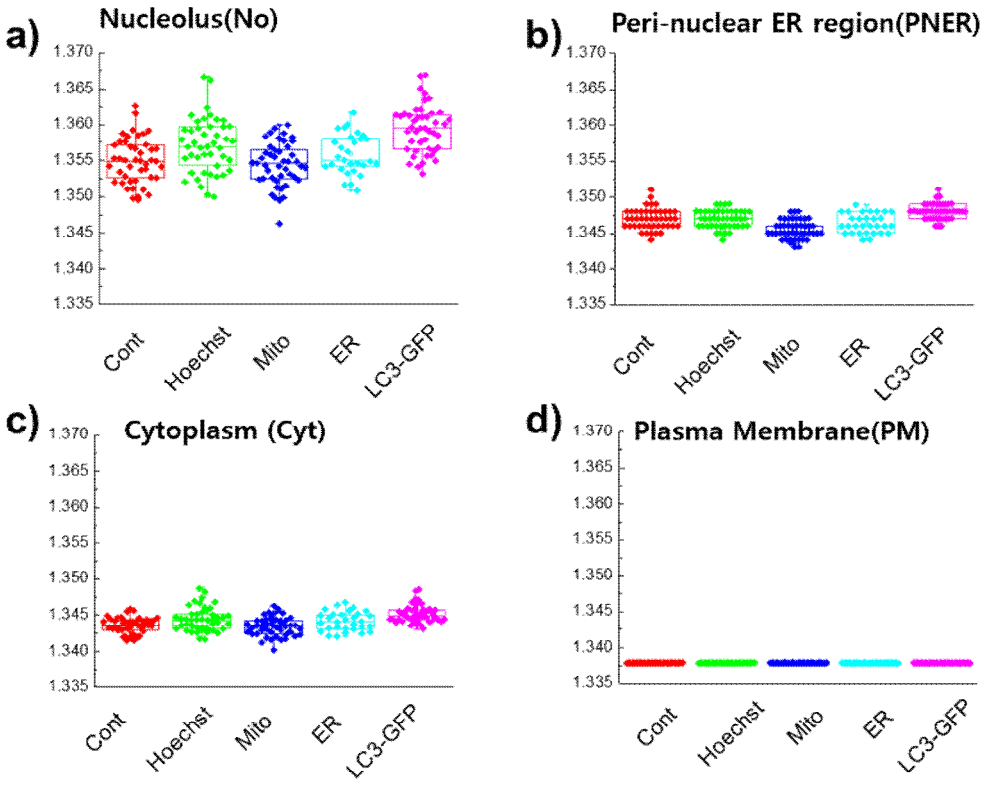

Figure 9. The refractive index (RI) values of four different cellular organelles in live HeLa cells with various fluorescence organelle tracker and transient LC3-GFP expression cell The average RI values of the nucleolus surrounded by the nuclear membrane (NO), the dense perinuclear region where the endoplasmic reticulum (ER) and mitochondria overlap (PNER), the cytoplasm (Cyt), and the cell plasma membrane (PM) are shown in separate panels.

Table 3. Summary of mean value for various treatment applied on HeLa cell

Cell condition	Nucleolus	ER	Cytosol	Cell membrane
37℃ DMEM (Live)	1.3561±0.0005	1.3461±0.0004	1.3438±0.0002	1.3379±0
25℃ PBS (Live)	1.3558±0.0004	1.3450±0.0003	1.3435±0.0003	1.3379±0
25℃ PBS (Fixed)	1.3542±0.0011	1.3431±0.0002	1.3423±0.0002	1.3379±0
TF(live) (unexpressed B23)	1.3552±0.0005	1.3453±0.0003	1.3441±0.0002	1.3379±0
TF (live) (expressed B23)	1.3567±0.0006	1.3459±0.0005	1.3439±0.0004	1.3379±0
TF (live) (expressed Lamin A)	1.3562±0.0005	1.3456±0.0003	1.3441±0.0002	1.3379±0
TF (live) (expressed EGFR)	1.3558±0.0007	1.3461±0.0004	1.3437±0.0003	1.3379±0
TF (live) (Expressed mGFP)	1.3583±0.0008	1.3483±0.0004	1.3455±0.0005	1.3379±0
TF (live) (Expressed mGFP+B23)	1.3590±0.0015	1.3485±0.0007	1.3454±0.0006	1.3379±0
HeLa / Hoechst	1.3554±0.0008	1.3460±0.0004	1.3441±0.0003	1.3379±0
HeLa / ER tracker	1.3558±0.0006	1.3461±0.0003	1.3442±0.0003	1.3379±0
HeLa/Mito tracker	1.3548±0.0003	1.3453±0.0004	1.3432±0.0004	1.3379±0
HeLa / LC3-GFP	1.3597±0.0029	1.3489±0.0009	1.344897±0.0009	1.3379±0

4. Discussion

In this study, hLD-SCs, hUCM-MSCs, and hiPSC were compared to fibroblasts, showing that refractive index and ODT can provide a 3D distribution of different density regions. hLD-SC and hUCM-MSC had a high number of vesicles and a large volume, and it was observed that vesicles with a large volume were widely distributed. The mean refractive index (RI) value of vesicles in hLD-SC, hiPSC, and hUCM-MSC was higher compared to that of vesicles in fibroblasts. Additionally, the presence of widely distributed large-volume vesicles indicated that these characteristics were unique to these three types of stem cells.(Figure 3, Table 2). For HeLa cell, various cell manipulation and external changes applying on cell were evaluated. Temperature increase and cell fixation decreased the organelle density, while cell membrane perforation lost most of the soluble components in the cytoplasm but showed minimal loss in the cell nucleus. According to RI value summaries shown in Figure 5, the RI values of PBS solution increased as temperature decreased, but small organelles such as NO and PNER showed relatively large increases, while the RI values of larger organelles such as cyt and PM increased to the same value as the PBS RI solution. Chemically fixed cells showed little morphological changes, but the overall density of the cells decreased and the density of the cytosolic region was low. This phenomenon is believed to be a result of increased cell permeability caused by the presence of 0.1% Triton X-100. This increased permeability leads to the release of molecules from the cytosol. In HeLa cells immune-stained with HSF4, the detection of the cytosolic density was impossible due to the increased cell permeability caused by 0.1% Triton X-100, and the density of PNER decreased, but the normal distribution of nuclear proteins was confirmed. Therefore, it was confirmed that the effect of cell permeability did not affect the morphology or location of cellular organelles, but caused significant loss of components in the cytosol and overall density decrease. In addition, the effects of genetic cell manipulation and chemical fluorescent staining were also investigated. Overexpression using genetic GFP

or GFP-tagged proteins increased the organelle density depending on the type of tagged protein. Interestingly, significant changes in cell volume and density were observed in cells where proteins were stably overexpressed. On the other hand, fluorescent trackers for specific organelle staining did not have a significant impact on cellular density. Figure 6 and Figure 8 represents morphology of HeLa cell after each treatment applied and Table 3 summarizes the RI value of each HeLa with gene overexpression and various tracker. To review HeLa cell with gene transfection, morphology of HeLa cell did not change much However, there was a change in the RI value. When comparing mRFP-expressing cells to non-expressing HeLa cells from the same cell line, an increase in RI values was observed in the nucleolus and PNER regions of the mRFP-expressing cells, but there was no significant difference in the cytosol. For Lamin A, EGFR-GFP, and GFP proteins, the region of high fluorescence intensity corresponded well with the region of high refractive index in each specific organelle. For HeLa cells transfected with both mGFP and mRFP B23, a significant increase in RI was observed in all cellular organelles. On the other hand, although there were no morphology changes in organelles in cells treated with organelle tracker, there was no change in the refractive index within the cellular organelles either. Figure 8 confirms that there were no changes in the raw ODT images of HeLa cells treated with Tracker. However, for HeLa cells continuously expressing LC3-GFP, colony formation was observed in multiple cells, and overall, an increase in RI values was also observed. HeLa cells expressing LC3-GFP protein exhibited high RI values in both the nucleolus, PNER, and cytosol, indicating that, similar to when various genes such as mGFP, EGFR-mGFP, Lamin A and mRFP were transfected into HeLa cells, the inserted gene also caused changes in intracellular organelle density.

5. Conclusion

Label-free ODT technology was used to evaluate the RI values and volumes of various stem cells compared to fibroblasts, and the effect of traditional cell manipulation on single HeLa cell molecules was also examined. Three types of stem cells (hLD-SCs, hUCM-MSCs, and hiPSC) were compared to fibroblasts using ODT correlated with fluorescent microscopy, revealing that stem cells had widely distributed vesicles with larger volumes and higher mean RI values than fibroblasts. This significant difference indicates that stem cells have unique characteristics compared to fibroblasts. In HeLa cells, various treatments resulted in differences in the RI values of each organelle. Temperature changes and Triton X-100 treatment caused changes in the cytoplasmic RI value, while gene overexpression (mGFP, LaminA, mRFP) resulted in high densities within the nucleolus, PNER, and cytoplasm of HeLa cells. Cell trackers had little effect on cell density or morphology. These findings emphasize the importance of the effects of treatment conditions on cellular composition when using invasive cell manipulation methods for biological and biochemical analysis of organoids using fluorescent microscopy or ODT. This study provides valuable information for developing less invasive cell manipulation methods and fluorescent probe designs for organoids, as well as for observing various cells in a label-free and live state

6. References

1. Pack C, Saito K, Tamura M, Kinjo M. Microenvironment and effect of energy depletion in the nucleus analyzed by mobility of multiple oligomeric EGFPs. Biophys J. 2006;91(10):3921-3936. doi:10.1529/biophysj.105.079467

2. Sako Y, Hiroshima M, Pack CG, Okamoto K, Hibino K, Yamamoto A. Live cell single-molecule detection in systems biology. Wiley Interdiscip Rev Syst Biol Med. 2012;4(2):183-192. doi:10.1002/wsbm.161

3. Park H, Han SS, Sako Y, Pack CG. Dynamic and unique nucleolar microenvironment revealed by fluorescence correlation spectroscopy. FASEB Journal. 2015;29(3):837-848. doi:10.1096/fj.14-254110

4. Wolf, E.. Optics Communications, 1969,1(4) 153-156.

5. Designed Research; Y SSP, Performed Research; G WCP. Contributed New Reagents/ Analytic Tools. Vol 105.; 2008.

6. Jung J, Kim K, Yoon J, Park Y. High-Fidelity Optical Diffraction Tomography of Multiple Scattering Sample. Opt Express. 2016;24(3):2006. doi:10.1364/oe.24.002006

7. Jung J, Kim K, Yoon J, Park Y. Hyperspectral optical diffraction tomography. Opt Express. 2016;24(3):2006. doi:10.1364/oe.24.002006

8. Jung JH, Hong SJ, Kim HB, et al. Label-free non-invasive quantitative measurement of lipid contents in individual microalgal cells using refractive index tomography. Sci Rep. 2018;8(1). doi:10.1038/s41598-018-24393-0

9. Kim YS, Lee S, Jung J, et al. Combining Three-Dimensional Quantitative Phase Imaging and Fluorescence Microscopy for the Study of Cell Pathophysiology. Vol 91.; 2018.

10. Kim TK, Lee BW, Fujii F, Kim JK, Pack CG. Physicochemical properties of nucleoli in live cells analyzed by label-free optical diffraction tomography. Cells. 2019;8(7).

11. Kim Y, Kim TK, Shin Y, et al. Characterizing Organelles in Live Stem Cells Using Label-Free Optical Diffraction Tomography. Mol Cells. 2021;44(11):851-860.

12. Kim SY, Lee JH, Shin Y, et al. Label-free imaging and evaluation of characteristic properties of asthma-derived eosinophils using optical diffraction tomography. Biochem Biophys Res Commun. 2022;587:42-48.

13. Pack CG. Application of quantitative cell imaging using label-free optical diffraction tomography. Biophys Physicobiol. 2021;18:244-253. Published 2021 Oct 15.

14. Yu KP, Lee GWM, Lin SY, Huang CP. Removal of bioaerosols by the combination of a photocatalytic filter and negative air ions. J Aerosol Sci. 2008;39(5):377-392.

15. Kim K, Park WS, Na S, et al. Correlative three-dimensional fluorescence and refractive index tomography: bridging the gap between molecular specificity and quantitative bioimaging. Biomed Opt Express. 2017;8(12):5688.

16. Guo R, Barnea I, Shaked NT. Limited-angle tomographic phase microscopy utilizing confocal scanning fluorescence microscopy. Biomed Opt Express. 2021;12(4):1869.

17. Herrera MB, Bruno S, Buttiglieri S, et al. Isolation and Characterization of a Stem Cell Population from Adult Human Liver. Stem Cells. 2006;24(12):2840-2850.

18. Najimi M, Khuu DN, Lysy PA, et al. Adult-Derived Human Liver Mesenchymal-Like Cells as a Potential Progenitor Reservoir of Hepatocytes? Cell Transplant. 2007;16:717-728.

19. Pan Q, Fouraschen SMG, Kaya FSFA, et al. Mobilization of hepatic mesenchymal stem cells from human liver grafts. Liver Transplantation. 2011;17(5):596-609.

20. Choi M, Ban T, Rhim T. Therapeutic use of stem cell transplantation for cell replacement or cytoprotective effect of microvesicle released from mesenchymal stem cell. Mol Cells. 2014;37(2):133-139.

21. Terasaki M, Loew L, Lippincott□Schwartz J, Zaal K. Fluorescent Staining of Subcellular Organelles: ER, Golgi Complex, and Mitochondria. Curr Protoc Cell Biol. 1998;00(1).

22. Su JW, Hsu WC, Tjiu JW, Chiang CP, Huang CW, Sung KB. Investigation of influences of the paraformaldehyde fixation and paraffin embedding removal process on refractive indices and scattering properties of epithelial cells. J Biomed Opt. 2014;19(7):075007.

23. Baczewska M, Eder K, Ketelhut S, Kemper B, Kujawińska M. Refractive Index Changes of Cells and Cellular Compartments Upon Paraformaldehyde Fixation Acquired by Tomographic Phase Microscopy. Cytometry Part A. 2021;99(4):388-398.

24. Cytochemistry and, Fox CH, Johnson FB, Whiting J, Roller PP. The Journal of Histochemistry Formaldehyde Fixation Review Article. Vol 33.; 1985.

25. Hua K, Ferland RJ. Fixation methods can differentially affect ciliary protein immunolabeling. Cilia. 2017;6(1).

26. Kabeya Y, Mizushima N, Ueno T, et al. LC3, a mammalian homologue of yeast Apg8p, is localized in autophagosome membranes after processing. EMBO Journal. 2000;19(21):5720-5728.

27. So S, Lee Y, Choi J, et al. The Rho-associated kinase inhibitor fasudil can replace Y-27632 for use in human pluripotent stem cell research. PLoS One. 2020;15(5).

28. Kim S, Lee SK, Kim H, Kim TM. Exosomes secreted from induced pluripotent stem cell-derived mesenchymal stem cells accelerate skin cell proliferation. Int J Mol Sci.

29. Lee Y, Kim T, Lee M, et al. De Novo Development of mtDNA Deletion Due to Decreased POLG and SSBP1 Expression in Humans. Published online 2021.

30. Merath K, Ronchetti A, Sidjanin DJ. Functional analysis of HSF4 mutations found in patients with autosomal recessive congenital cataracts. Invest Ophthalmol Vis Sci. 2013;54(10):6646-6654.

31. Meder VS, Boeglin M, de Murcia G, Schreiber V. PARP-1 and PARP-2 interact with nucleophosmin/B23 and accumulate in transcriptionally active nucleoli. J Cell Sci. 2005;118(1):211-222.

32. Chen D, Huang S. Nucleolar Components Involved in Ribosome Biogenesis Cycle between the Nucleolus and Nucleoplasm in Interphase Cells. Vol 153.; 2001.

33. Campbell RE, Tour O, Palmer AE, et al. A Monomeric Red Fluorescent Protein.

34. Yasui M, Hiroshima M, Kozuka J, Sako Y, Ueda M. Automated single-molecule imaging in living cells. Nat Commun. 2018;9(1).

35. Kim G, Lee M, Youn SY, et al. Measurements of three-dimensional refractive index tomography and membrane deformability of live erythrocytes from Pelophylax nigromaculatus. Sci Rep. 2018;8(1).

36. Kim TK, Lee BW, Fujii F, et al. Mitotic chromosomes in live cells characterized using high-speed and label-free optical diffraction tomography. Cells. 2019;8(11).

37. Reisler E, Eisenberg H, Minton AP. Temperature and density dependence of the refractive index of pure liquids. Journal of the Chemical Society, Faraday Transactions 2: Molecular and Chemical Physics. 1972;68:1001-1015.

38. Khodier SA. Refractive Index of Standard Oils as a Function of Wavelength and Temperature. Vol 34.; 2002.

39. Jiao X, Khan SY, Kaul H, et al. Autosomal recessive congenital cataracts linked to HSF4 in a consanguineous Pakistani family. PLoS One. 2019;14(12).

40. Huang S, Xu X, Wang G, et al. DNA Replication Initiator Cdc6 Also Regulates Ribosomal DNA Transcription Initiation.; 2016.

41. Finch RA, Revankar GR, Chan PK. Nucleolar localization of nucleophosmin/B23 requires GTP. Journal of Biological Chemistry. 1993;268(8):5823-5827.

42. Cheng R, Zhang F, Li M, Wo X, Su YW, Wang W. Influence of Fixation and Permeabilization on the Mass Density of Single Cells: A Surface Plasmon Resonance Imaging Study. Front Chem. 2019;7.

43. Shimi T, Pfleghaar K, Kojima SI, et al. The A- and B-type nuclear lamin networks: Microdomains involved in chromatin organization and transcription. Genes Dev. 2008;22(24):3409-3421.

44. Tanaka T, Zhou Y, Ozawa T, et al. Ligand-activated epidermal growth factor receptor (EGFR) signaling governs endocytic trafficking of unliganded receptor monomers by non-canonical phosphorylation. Journal of Biological Chemistry. 2018;293(7):2288-2301.

45. Ni HM, Bockus A, Wozniak AL, et al. Dissecting the dynamic turnover of GFP-LC3 in the autolysosome. Autophagy. 2011;7(2):188-204.

46. Kaizuka T, Morishita H, Hama Y, et al. An Autophagic Flux Probe that Releases an Internal Control. Mol Cell. 2016;64(4):835-849.

국문요약

광학 회절 단층촬영(ODT) 기술은 형광 라벨이나 다른 전처리 없이 세포와 세포 소기관을 관찰할 수 있는 무표지 관찰 기술입니다. 이 기술은 기존의 세포 이미징 기술인 형광 현미경이나 전자 현미경의 한계를 극복합니다. 예를 들어, 형광 현미경이나 전자 현미경은 2차원 이미지를 제공하며 세포를 고정시키고 면역화학 염색이나 형광 유전자 발현 등의 전처리가 필요합니다. 이는 세포 내 물리화학적 조성에 변화를 일으킬 수 있습니다. 반면 ODT는 세포 전처리 없이 3차원 세포 및 세포 소기관 이미지를 제공하며, 굴절률, 부피, 무게 등과 같은 물리적 매개변수도 제공합니다. 따라서 ODT를 이용하면 세포 내 미세 환경 변화 및 내부 생물학적, 물리학적 특징을 분석할 수 있습니다. 또한 ODT로 세포를 관찰할 때 무표지 라이브 세포 뿐만 아니라 세포 고정, 유전자 변형, 면역 형광 및 생물 표지자를 사용한 다양한 전처리가 가능합니다. 무표지 라이브 세포와 다양한 전처리를 받은 세포는 형태와 내부 구성이 다르며, 이러한 변화를 수치 값으로 변환하여 굴절률 렌더링을 통해 양적으로 평가할 수 있습니다. ODT의 이점을 활용하여 세포를 관찰하면, 라이브 상태에서 유사한 세포 범주 간의 물리적 특성 차이를 구별할 수 있을 뿐 아니라 세포 내의 특정 표지자를 라벨링하여 내부 변화를 수치적으로 평가할 수 있습니다. 본 연구에서는 인간 줄기세포, 섬유아세포 및 HeLa 세포의 굴절률과 부피를 ODT를 이용하여 측정하였습니다. 또한 온도, 세포 고정, GFP 단백질 표시, 세포 소기관 추적 등 다양한 물리적 자극에 의한 굴절률의 차이도 비교하였습니다. 줄기 세포의 경우 hLD-SCs, hUCM-MSCs 및 hiPSC와 같은 세 가지 종류의 줄기세포를 배양하여 섬유아세포와 비교하였습니다. 분석결과, 줄기세포들은 섬유아세포와 비교하여 훨씬 넓게 분포된 소포를 가지며, 이 소포들은 더 큰 부피와 높은 평균 굴절률(RI) 값을 가지고 있음을 확인하였습니다. 이러한 결과는 줄기세포가 섬유아세포와 비교하여 소포의 분포, 부피 및 굴절률 값 등에서 독특한 특성을 가지고 있음을 나타냅니다. HeLa 세포에 다양한 전처리 후 비교하는 실험결과로는 세포 고정 및 온도 상승 후, 핵과 세

포질과 같은 소기관의 굴절률(RI) 값이 전반적으로 크게 감소하는 것을 발견했습니다. 또한, GFP 및 GFP-단백질의 발현이 세포 소기관의 굴절률(RI) 값을 화학적 형광 염색으로 얻은 것보다 유의하게 증가시킴을 보여주었습니다. 이처럼 ODT는 특정 생물학적 마커가 필요 없이 세포 간 차이를 파악할 수 있도록 해주며, 외부 자극이 세포 소기관에 미치는 영향을 간접적으로 평가할 수 있습니다. 이러한 정보는 다른 전통적인 현미경 기술을 이용한 미래 연구에 참고 자료로 활용될 수 있습니다.